Chronology of alluvial terrace sediment accumulation and incision in the Pativilca Valley, western Peruvian Andes

Camille Litty[1*], Fritz Schlunegger[1], Naki Akçar[1], Romain Delunel[1], Marcus Christl[2], Christof Vockenhuber[2]

[1] *Institute of Geological Sciences, University of Bern, Baltzerstrasse 1+3, CH- 3012 Bern.*

[2]*Laboratory of Ion Beam Physics, ETH Zurich, Zurich, Switzerland*

* *Current address: Univ. Grenoble Alpes, IUGA, ISTerre, 38000 Grenoble, France*

ABSTRACT

The incision and aggradation of the Pativilca alluvial fan delta system in the western Peruvian Andes through Quaternary time can be traced in detail using well-exposed fill terraces studied by a combination of cosmogenic nuclide dating, terrace mapping and paleo-erosion rate calculations. Two alluvial terraces have been dated through depth-profile exposure dating using in-situ ^{10}Be. The dating results return an age for the abandonment of the terrace at 200 ± 90 ka in Pativilca and 1.2 Ma ± 0.3 Ma in Barranca. These new ages complete the database of previously dated terrace fills in the valley. Together with the results of the terrace mapping and the absolute ages of the terraces, we show that the valley fills are made up of at least four terraces; two terraces near the city of Pativilca and two terraces in the city of Barranca. While previous studies have shown two periods of sediment aggradation, one period around 100 ka (Barranca) and another period around 30 ka (Pativilca), our new results show two additional periods of sediment aggradation and subsequent incision that have not been reported before. Finally, paleo-erosion rates at the time of the deposition of the terrace material were calculated and compared to the available modern estimates. The paleo-erosion rates vary from 140 ± 12 m/Ma to 390 ± 40 m/Ma. The period of sediment accumulation prior to the abandonment of the terrace at 200 ka corresponds to a wet phase and a pulse of erosion. In contrast, the period of sediment accumulation prior to the abandonment of the terrace at 1.2 Ma does not

correspond to a pulse of erosion and could rather correspond to a change of the base level possibly induced by a sea-level rise.

Keywords: ^{10}Be depth-profile dating; alluvial terraces; Pativilca Valley; Western Peruvian Andes

1. Introduction

Fluvial sediments originating from mountain belts like the Andes yield important archives of past environmental or tectonic changes. The sediments can record changes in precipitation rates and climate (Litty et al., 2016; d'Arcy et al., 2017). They can also record the response to earthquake-induced landslides (McPhillips et al., 2014). The reconstruction of the timing of alluvial sediment deposition thus bears important information when the scope lies in the detection of specific climate or tectonic events as driving forces of landscape evolution. In this context, depth-profile dating based on in-situ produced ^{10}Be measured in quartz has been proven a reliable method to establish a chronology of sediment deposition (e.g., Bookhagen et al., 2006; Hidy et al., 2010). In particular, this methodology yields an age when sediment aggradation stopped and when a period of sediment accumulation was superseded by a phase of erosion and incision into the previously deposited material. ^{10}Be is the most commonly measured in situ–produced cosmogenic nuclide (Granger et al., 2013). Its dominance in geological applications stems from several factors, including the abundance of the target mineral, quartz, a standardized chemistry procedure (Kohl and Nishiizumi, 1992), a relatively simple production depth profile, and routinely good precision by accelerator mass spectrometry (AMS) (Granger, 2006). Additionally, isochron burial dating using ^{10}Be and ^{26}Al is becoming increasingly important in studies related to river terraces (e.g., Darling et al., 2012; Erlanger et al., 2012; Akçar et al., 2017). Isochron-burial dating yields in an age when the investigated material accumulated. It is thus a variation of traditional burial dating methods. Ages, or alternatively the burial times of sediment, are determined using the difference between the cosmogenic ^{26}Al/^{10}Be surface production ratio at the time of burial and the ^{26}Al/^{10}Be ratio measured in buried sediments (Granger, 2006). Sediments of alluvial terrace deposits with flat tops are ideal for surface exposure dating and isochron burial dating: they are persistent, easily identifiable as surfaces that were formed at a specific time and that have been isolated from the fluvial system since deposition. Because they

53 are typically coarse-grained, well drained, and nearly flat, they can be remarkably well preserved and
54 unaffected by erosion, especially in arid environments like in the western side of the Peruvian Andes
55 (Litty et al., 2017a; Reber et al., 2017).

56 Alluvial terrace sequences are common features along the coastal margin between Peru and
57 northern Chile. They are located particularly in lower valley reaches near to the Pacific coast (Steffen
58 et al., 2009, 2010; Trauerstein et al., 2014; Litty et al., 2017a). Climate change has been considered to
59 have controlled pulses of erosion on the western Andean margin through the increase in mean surface
60 runoff resulting either in sediment accumulation along stream segments close to the Pacific coast
61 (Bekaddour et al., 2014; Norton et al., 2016), or in surface erosion in upstream segments of major
62 rivers (Veit et al., 2016). These climate-driven changes have been interpreted as being the main
63 driving force controlling the sediment accumulation and the formation of cut-and-fill terraces on the
64 western Andean margin (Norton et al., 2016). In the Pativilca Valley, situated on the western margin
65 of the Peruvian Andes at about 10°S (Fig. 1A), a terrace sequence has been previously dated through
66 infrared stimulated luminescence (IRSL) techniques (Trauerstein et al., 2014). The results have
67 disclosed the occurrence of at least two periods of sediment aggradation, one period spanning from 10
68 ka to 90 ka with an age of the samples cluster around 30 ka and another period spanning the time
69 interval between 80 ka and 130 ka with an age estimate of the samples cluster around 110 ka
70 (Trauerstein et al., 2014). While generally wetter climate results in fluvial incision, the results from
71 Trauerstein et al. (2014) suggested that here wetter climate conditions do correlate with periods of
72 fluvial aggradation.

73 The aim of this study is to date additional terrace deposits using in-situ terrestrial cosmogenic
74 nuclides to complete the chronological framework and to infer the history of sediment aggradation
75 and incision in this alluvial fan delta system. In addition concentrations of in-situ ^{10}Be recorded by
76 detrital quartz minerals in the terrace deposits will be used to infer the paleo-erosion rates recorded at
77 the time when sediment accumulation occurred. These rates will be compared to the modern ones
78 (Reber et al., 2017) to quantify the erosion in the upstream drainage basin during the phases of
79 aggradation within the downstream valley. The final aim is to understand the factors controlling
80 fluvial aggradation and incision in fan delta environments in the western Andes.

2. Regional settings

The Pativilca Valley is located in central Peru, about 200 km to the northwest of Lima. The Rio Pativilca, which is trunk stream of the region, debouches into the Pacific at 10.7°S and 77.8°W (Fig. 1A). The drainage basin has an area of about 4400 km^2, and the longest flow path measures approximately 200 km. The upper section of the stream is characterized by a bedrock channel with a steep gradient (knickzone), whereas in the lower segment the narrow valley floor is covered by alluvial deposits that are thickening and widening towards the coast, giving way to an alluvial fan delta. The sedimentological architecture of the deposits is characterized by amalgamated stacks of 20 to 50 m-thick units of poorly sorted, clast-supported conglomerates with a coarse-grained sandy matrix (Fig. 1B). The clasts are subrounded and sometimes imbricated, but the sedimentary fabrics are predominantly massive (Fig. 1B). The alluvial conglomerates are part of an alluvial fan delta system characterized by a suite of individual fill terraces with different altitudes of the tread (Fig. 1B).

The precipitation pattern of South America is strongly influenced by the low level Andean jet and the position of the Inter Tropical Convergence Zone (ITCZ), which experiences seasonal shifts in response to insolation differences between austral summer and winter. The Andean jet transfers humidity from the Pacific Ocean and the Amazon basin to the eastern margin of the Andes, and also to the Altiplano and the western Andean margin (Garreaud, 2009). The Andean mountain range thus acts as a major topographic barrier to the atmospheric circulation. As a result of this circulation pattern, the Peruvian western margin shows an E-W contrasting precipitation pattern with high annual precipitation rates up to 800 mm on the Altiplano and ~0 mm along the coast. From north to south, the annual rainfall rates on the Altiplano decrease from 1000 mm near the Equator to <200 mm in northern Chile. Every 2-10 yr, near the Equator, the Pacific coast is subjected to stronger precipitation than the mean precipitation rates, resulting in high flood magnitude variability related to the El Nino Southern Oscillation (ENSO) weather phenomenon (DeVries, 1987). Today, this phenomenon is limited to the coastal area of northern Peru, but during the past, southern Peru might also have been affected by such events (Lagos et al., 2008).

On orbital time scales, the position of the ITCZ has shifted in response to larger insolation and heat contrasts between the Northern and Southern Hemispheres, which has been related to the effects of shifts in the Earth's precession (Strecker et al., 2007). The results are stronger upper air easterlies and more precipitation on the Altiplano (Garreaud et al., 2003). Variations in precipitation rates and patterns led to remarkable lake level variations on the Altiplano as recorded by lake level highstands on the plateau (Ouki, Minchin and Tauca pluvial periods, e.g., Fritz et al., 2004). These climate changes have also controlled pulses of erosion and deposition on the western Andean margin (Bekaddour et al., 2014; Veit et al., 2016). Related variations in erosional fluxes have been interpreted as being the main factor controlling the formation of cut-and-fill terrace systems along the western margin of the Peruvian Andes (Norton et al., 2016).

3. Methods

3.1. Cosmogenic nuclides

Over the past 25 yr, cosmogenic nuclides have become an essential tool in Quaternary geochronology (e.g., Gosse and Phillips, 2001; Granger, 2006). Cosmogenic nuclides are produced through spallation reactions and muon capture in minerals of rocks and sediment at or near the Earth's surface (Gosse and Philips, 2001). Cosmogenic ^{10}Be and ^{26}Al can be applied to determine a post-depositional age of a geological layer using their accumulation (depth-profile dating). Alternatively, they can also be used to determine the timing of sediment accumulation through their radioactive decay (burial dating) history (e.g., Anderson et al., 1996; Repka et al., 1997; Granger and Smith, 2000; Granger and Muzikar, 2001; Wolkowinsky and Granger, 2004; Balco and Rovey, 2008; Akçar et al., 2017).

Depth-profile dating is based on the exponential decrease of cosmogenic nuclides with depth (Gosse and Philips, 2001). On the other hand, the burial dating technique uses the difference in half-lives of ^{10}Be (1.387 Ma; Korschinek et al., 2010; Chmeleff et al., 2010) and ^{26}Al (0.705 Ma; Norris et al., 1983) and thus the ^{26}Al versus ^{10}Be ratio to determine the burial time, when the pre-burial and post-burial concentrations are known or estimated (e.g., Granger and Muzikar, 2001; Akçar et al.,

2017). We followed the Erlanger et al. (2012) isochron approach where one of the advantages is the assumption that post-burial production is identical across a single stratigraphic horizon.

The collected samples (see section 3.3 for description of sample sites and sampling strategy) were processed in the Surface Exposure Laboratory of the Institute of Geological Sciences at the University of Bern following the lab protocol described in Akçar et al. (2012). The $^{10}Be/^{9}Be$ and $^{26}Al/^{27}Al$ AMS measurements were then performed at the Swiss Federal Institute of Technology tandem facility in Zurich (Christl et al., 2013). The long-term weighted average $^{10}Be/^{9}Be$ ratio of $(2.41 \pm 0.53) \times 10^{-15}$ was used for full process blank correction. Table 1 presents the samples information and cosmogenic nuclide results.

Depth-profile ages were modelled with MATLAB® using Monte Carlo simulations developed by Hidy et al. (2010). Depth-profile patterns were simulated based on exposure age, erosion rate and inheritance. Table 2 shows the input parameters for the Barranca and Pativilca depth-profile simulations. We applied no correction factor for topographic shielding. We justify this approach because there is no significant topography around the sampling sites that could block a portion of incoming cosmic radiations (Dunne et al., 1999; Gosse and Phillips, 2001), as the sampling sites are located on the widest and flattest part of the valley close to the coast. We did not consider snow cover to have a major impact on the results as the mean basin elevation of the sampled catchment is largely situated below the snow line. The ^{10}Be half-life with a value of 1.387 ± 0.012 Ma was utilized (Chmeleff et al., 2010; Korschinek et al., 2010). The local production rate was scaled to the Lal (1991) and Stone (2000) scheme using a production rate caused by spallation (SLHL: at sea-level, high latitude) of 4.01 ± 0.12 atoms g_{SiO2}^{-1} (CRONUS calculator update from v. 2.2 to v. 2.3 published by Balco in August 2016 after Balco et al., 2008; Borchers et al., 2016). Thus a site-specific spallogenic production rate of 2.5 ± 0.5 atoms g^{-1} a^{-1} was obtained for Barranca and for Pativilca. We applied a bulk density ranging between 1.6 and 2.1 g cm^{-3} for the sediment samples in Barranca and Pativilca. Finally, to model a depth-profile age we simulated 100,000 profiles and used a $\chi 2$ cut-off value of ≤ 20 for Barranca and ≤ 3 for Pativilca (Table 2).

3.2. Paleo erosion rates

163 Paleo basin-averaged erosion rates can be calculated using the cosmogenic nuclide
164 concentrations of past sediment samples following Granger et al. (1996) and von Blanckenburg
165 (2005). To calculate the basin averaged paleo-erosion rate, we used the ^{10}Be cosmogenic nuclide
166 concentrations of the sand embedded in the terrace deposits after corrections have been made for
167 shielding, post-depositional nuclide production at sample depth *z*, and atom loss due to radioactive
168 decay during time *t* (both considered in Eq. (1); Balco et al., 2008). These equations can be used
169 assuming: (i) The material was well mixed in the upstream basin and finally embedded in the terrace
170 fill. This appears to be the case in the western Peruvian valleys where the fluvial processes have
171 dominated the transport of sediment (Litty et al., 2017b), thus providing well-mixed material. (ii) The
172 paleo-erosion is representative for the entire catchment. Indeed, the sediments of the Pleistocene
173 terrace fills in western Peru record an origin from both the upper flat part of the catchments and the
174 lower steep reaches (Litty et al., 2017a). (iii) The residence of the material on the hillslopes and the
175 channels is much shorter than the erosional timescale. This is the case in the western Peruvian valleys
176 where regolith was considered to have been rapidly stripped from hillslopes, which most likely
177 resulted in the supply of large volumes of sediment to the trunk streams during the periods of
178 sediment aggradation (Norton et al., 2016). (iv) The individual terraces have not experienced multiple
179 phases of erosion and re-deposition, so that major internal unconformities are not present (von
180 Blanckenburg, 2005). This appears to be the case in the Pativilca Valley as no unconformities in the
181 individual terrace fills have been observed in the field.
182
183 *3.3. Sampling sites*
184 Two previously undated alluvial terrace fills were sampled for depth-profile exposure dating.
185 These terraces are located along the lowermost reach of the Pativilca River and in the city of Barranca
186 (Fig. 1; Table 1). At each sampling site, six samples were collected along a vertical profile from 0.9 to
187 4.7 m beneath the tread of the terrace in Pativilca, and from 0.4 to 3.2 m beneath the tread of the
188 terrace in Barranca (Fig. 1A). Two to three kilograms of medium grained sand embedded between the
189 pebbles were taken for each sample. Additionally, the lowermost samples of the two depth profiles
190 (PAT-DP6 and BAR-DP6) were used to infer a paleo-erosion rate at the time when the sediments of

191 the two newly dated terraces were deposited. Two other samples (PAT-PE and BAR-PE2) were
192 collected in two other terrace fills previously dated (Trauerstein et al., 2014) for the calculation of
193 paleo-erosion rates (one in Pativilca and one in Barranca; Table 4). Additionally, quartz bearing clasts
194 were sampled for isochron burial dating (Fig. 1B; Table 1). For each isochron burial site, the samples
195 were collected from the same sedimentologic unit and from a single stratigraphic horizon following
196 Erlanger et al. (2012). Three horizons were sampled in Barranca and two horizons have been sampled
197 in Pativilca (Fig. 1B; Table 1). Depth-profile dating and isochron burial dating techniques have be
198 chosen as sand lenses that are required for IRSL sampling are not present in every terrace fill.

199

200 **4. Results**

201 *4.1. Cosmogenic nuclides: isochron burial dating*

202 The measured ^{26}Al concentrations are plotted versus ^{10}Be concentrations including 2σ
203 uncertainties (Fig. 2). The cosmogenic nuclide results are shown in Table 1. As the Al/Be ratios are
204 higher than the surface ratio, it is not possible to calculate an isochron burial age from these samples
205 (for details, see Erlanger et al., 2012). The surface ratio of $^{26}Al/^{10}Be$ is not constant since it depends
206 on the time of exposure and erosion. On a banana-plot, the ratios decrease from 8.4 to ~3, and a
207 regression through these yields a surface ratio around 6.8. Therefore, in most of the isochron burial
208 applications this ratio has been used as the surface ratio. Recently, Akçar et al. (2017) showed that
209 this ratio varied between 7 and 12 in deeply eroding landscapes, particularly in glacial environments.
210 However, these mechanisms fail to explain the $^{26}Al/^{10}Be$ ratios > 12 obtained in this study as glacial
211 processes were most likely not the most important erosional mechanisms. Therefore, we tentatively
212 attribute these ratios to the analytical problems related to the measurements of the total Al or to the
213 quartz purification process. Given that no age can be determined from these samples; isochron burial
214 dating is therefore not further discussed in this paper.

215

216 *4.2. Cosmogenic nuclides: depth-profile dating*

217 *4.2.1. Barranca*

218 AMS-measured $^{10}Be/^{9}Be$ (with uncertainties) as well as calculated ^{10}Be concentrations for
219 each sample are shown in Table 1. The concentrations of the six sediment samples vary from ~12 x
220 10^5 atoms g^{-1} for the uppermost sample to ~1 x 10^5 atoms g^{-1} for the lowermost sample (Table 1). In
221 Fig. 3, the ^{10}Be concentrations together with 1σ uncertainties are plotted against depth. They display
222 an exponential decrease with depth. The simulated best fit curve through the six data points is
223 illustrated in Fig. 4, whereas the possible solution space with a $\chi 2$ cut-off value of ≤ 20 is shown in
224 Fig. 5.

225 The simulation yields a best-fit solution to the measured nuclide concentrations for a modal
226 depth-profile age of 1.2 ± 0.3 Ma, and a modal top erosion rate of 0.07 ± 0.02 cm ka^{-1} (Table 3A). The
227 modal values of the age and erosion rate are similar to the mean and median values of the simulation,
228 thus the errors of the modal values are based on the minimum and maximum values generated by the
229 simulation. Note that the Monte Carlo simulation code requires a constraint on the net erosion on the
230 top of the section as a modal input parameter to calculate an age (Hidy et al., 2010). This parameter is
231 iteratively adjusted within a range of values.

232

233 *4.2.2. Pativilca*

234 The concentrations of the six sediment samples vary from ~86 x 10^4 atoms g^{-1} for the
235 uppermost sample to ~44 x 10^4 atoms g^{-1} for the lowermost sample (Table 1). In Fig. 6, the ^{10}Be
236 concentrations together with 1σ uncertainties are plotted against depth. The best fit through the six
237 data points is illustrated in Fig. 7, whereas the possible solution space with a $\chi 2$ cut-off value of ≤ 3 is
238 shown in Fig. 8.

239 The simulation yields a best-fit solution to the measured nuclide concentrations for a modal
240 depth-profile age of 200 ± 90 ka, a modal top erosion of 0.48+ 0.41- 0.13 cm ka^{-1} and an inheritance
241 of 35,100+ 8700-8000 atoms g^{-1} (Table 3B). The modal values are similar to the mean and median
242 values of the simulation, thus the errors of the modal values are based on the minimum and maximum
243 values generated by the simulation.

The results of the depth-profile dating return a surface exposure age of ~1.2 Ma in Barranca and of ~200 ka in Pativilca. These results show minimum ages when the accumulation of material has terminated and when dissection of the previously deposited material started, yielding in the formation of a terrace level. These two periods when sediment aggradation was superseded by dissection, have not been dated before. These new results together with the ones from Trauestein et al. (2014) suggest the occurrence of at least four terraces referred to as T1 to T4 from older to younger (Figs. 9 and 10A), corresponding to at least four different periods of sediment accumulation. Terrace deposits were correlated on the basis of landscape position, tread altitude and absolute dating (Figs. 9 and 10A).

4.3. Paleo-erosion rates

The in-situ ^{10}Be analytical data together with the inferred paleo-erosion rates recorded by the alluvial terrace sediments are presented in Table 4. The paleo-erosion rate values are 143 ± 12 m Ma^{-1} at the time of the accumulation of the terrace deposits T1 (~1.2 Ma ago), 302 ± 28 m Ma^{-1} at the time when terrace material T2 was deposited, 392 ± 40 m Ma^{-1} at the time of the deposition of the terrace sediments T3, and finally 297 ± 29 m Ma^{-1} at the time terrace T4 was constructed (Fig. 10B). In addition, Reber et al. (2017) reported a modern catchment-averaged denudation rate of 260 ± 23 m Ma^{-1}.

5. Discussion

5.1. Chronology of sediment accumulation and incision

The fluvial aggradation and subsequent incision in the Pativilca Valley has occurred in multiple episodes through the Quaternary (Figs. 9 and 10). Figure 11 shows the position of the active river and the position of the sediment accumulation during the periods of aggradation. Our dating results imply that the sediments of terrace T1 in Barranca have been deposited prior to 1.2 Ma. The aggradation then ceased and the tread formation began ~1.2 Ma ago (terrace T1; Fig. 11A). During the period of the terrace fill, the erosion rate was two times lower than the modern rate (Fig. 12). Following this, for approximately 1 Ma, either a period of no sedimentation occurred in the valley or no sediments have been preserved. The river then moved its course towards Pativilca. The sediments

271 of terrace T2 in Pativilca have been deposited prior to 200 ka. The accumulation of sediment then
272 stopped and exposed the terrace tread at around 200 ka (terrace T2; Fig. 11B). During the period of
273 sediment accumulation, the erosion rate was up to ~300 m.Ma^{-1} (Fig. 12). The river bed again
274 changed its course towards Barranca, and a phase of accumulation occurred around 100 ka (deposition
275 of the sediment of T3; Fig. 11C; Trauerstein et al., 2014). In this period, the erosion rate was at its
276 highest (~400 m Ma^{-1}; Fig. 12). Finally, the lobe of the Pativilca fan delta moved back towards the
277 city of Pativilca close to its current course, and a phase of aggradation occurred from 10 to 45 ka ago
278 (deposition of the sediment of T4; Fig. 11D; Trauerstein et al., 2014). During this period, the
279 catchment-wide denudation rate dropped back to ~300 m Ma^{-1} (Fig. 12). This phase was followed by
280 a period of incision exposing the tread and riser of terrace level T4. Today the erosion rate is slightly
281 lower than during the past at ~200 ka (Fig. 12) and the river appears to be incising.
282
283 *5.2. Implications for climate variability as controls on cyclic deposition and erosion*
284 A stratigraphic record of river terrace sediments is formed and preserved as a stream changes
285 its activity between incision, lateral planation, and aggradation (Pederson et al., 2006). These fill
286 terraces in the Pativilca Valley represent a relatively complete archive of both incision and deposition.
287 They can be used to understand the response to climate or to other driving forces that have an impact
288 on the balance between sediment transport and deposition (Pederson et al., 2006). These terrace fills
289 have been formed in the alluvial fan delta of the Pativilca River and they might also record the change
290 in the position of the different lobes of the delta through shifts in transport and sediment capacity.
291 Alternatively, a phase of accumulation requires the availability of sediments on the hillslopes to be
292 eroded, transported and deposited (Hancock and Anderson, 2002). This implies that the river
293 experiences an increase in the ratio between sediment supply and the stream's capacity to control the
294 deposition the supplied material (Tucker and Slingerland, 1997). The youngest period of sediment
295 accumulation ranging from 10 to 45 ka (terrace T4) could correspond to the wet intervals recorded by
296 the Minchin (47.8–36 ka ago) and Tauca (26–14.9 ka ago) paleolakes (Fritz et al., 2004). The period
297 of sediment accumulation ranging from 80 to 130 ka (terrace T3) could correspond to the wet period
298 characterized by the Ouki paleolakes (120-98 ka ago; Fritz et al., 2004). These two periods of

sediment accumulation previously dated by Trauerstein et al. (2014) are thus correlated with phases of enhanced precipitation with higher water discharge in the river. These wet conditions could have been induced by summer insolation forcing of the South American summer monsoon at precessional time-scales (Baker et al., 2001a,b). Indeed, the precession together with the obliquity has been considered to control the seasonal cycles of insolation (Milankovitch, 1941). The wettest phases, and hence the highest lake levels (Bills et al., 1994; Sylvestre et al., 1999; Placzek et al., 2006), were additionally forced by warm North Atlantic sea surface temperatures (Baker et al., 2001a). These climate changes were also used to explain the pulses of upland erosion and deposition in the stream valleys on the western Andean margin (Bekaddour et al., 2014), which agree with our data of relative fast paleo-erosion rates recorded by these two terraces. Indeed, the 10-45 ka denudation rate was >10% higher than the modern one and the 80-130 ka denudation rate was even >30% higher than the modern rates (Fig. 12). Fluvial aggradation is here correlated with wetter climates and an increased sediment supply from the uplands. However, we also note that wetter climates can result in fluvial incision and terrace formation because of greater stream discharge (Veit et al., 2016), provided that the hillslopes have been depleted of material (Norton et al., 2016). In our case, the start of the incision phases could then correspond to the end of the pluvial period and the time of decrease of the supply of sediment to the river. Alternatively, it is also possible that erosional recycling of the terrace material started within the pluvial periods, when the preceding phase of rapid hillslope erosion resulted in the depletion of the sediment reservoirs, yielding high ratios between water and sediment fluxes in the trunk stream. The Altiplano lake sediment cores do not record climatic variations older than 130 ka (Placzek et al., 2006). In this context, we cannot correlate the two older periods of sediment accumulation (prior to ~200 ka and prior to ~1.2 Ma) to any lake level variations. However, the high paleo-erosion rate calculated for the newly dated fills of the terrace T2 (~15% higher than the modern one) appears also to correspond to a pulse of upland erosion, which could point towards a period of wet conditions. Support for this interpretation is provided by the periodicity of about 100 ka for this orbital-induced summer insolation forcing (Milankovitch, 1941; Lisiecki, 2010; Abe-Ouchi et al., 2013). If this interpretation is valid, then the ages of 100 ka (T3) and 200 ka (T2) would then correspond to this 100 ka periodicity, suggesting that the period prior to ~200 ka might also have corresponded to a wet

phase on the Altiplano. The oldest dated period of sediment accumulation (terrace T1) does not record a distinct pulse of erosion as the calculated paleo erosion rate was twice as low as the modern one. The production of sediments on the hillslopes through weathering and erosion can occur through an increase in precipitation rates (e.g., Bookhagen et al., 2005; Norton et al., 2016), for which there is no evidence from the records reported here indicating that sediment accumulation of the terrace T1 has not been induced by a phase of enhanced precipitation. Alternatively, this T1 phase of accumulation could have occurred in response to a rise in sea level. Indeed, a rise in sea level would cause a back filling and a super-elevation of the channel, which then would cause the delta lobe to switch positions. Supporting evidence for this interpretation has been provided by Pillans et al. (1998), who proposed that the ~1.2 Ma-old period was relatively warm and corresponded to a rising sea level. Nevertheless, we note that further research in the region is required to sustain this interpretation.

6. Conclusions

The results of the depth-profile dating together with the previously published IRSL ages (Trauerstein et al., 2014) disclose at least four terraces located in the fan delta of the Pativilca River. The sediments of terrace T1 accumulated until ~1.2 Ma ago and terraces T2, T3 and T4 were deposited prior to ~200 ka, ~100 ka ago and ~30 ka ago respectively. Additionally, paleo-erosion rates at the time of the deposition of the terrace fills were calculated and compared to the modern rates. The modern erosion rate is ~260 mm/ka, while the paleo-erosion rates vary from ~143 mm/ka to ~391 m Ma^{-1}.

The oldest period of accumulation does not correspond to a distinct pulse of erosion and could rather correspond to a period when the sea level was rising. The three younger phases of sediment accumulation most likely correspond to wet phases and pulses of erosion in the uplands. These wet conditions were likely to have been induced by summer insolation forcing of the South American summer monsoon at precessional time scales (Baker et al., 2001a, 2001b). Generally, wetter climate results in fluvial incision caused by greater stream discharge. However, wetter climate is here correlated with fluvial aggradation due to the inferred increased sediment supply from the uplands. The abandonment of the terrace treads would then correspond to the end of the pluvial period and thus

a decrease of the sediment supplied to the river. Additionally, this long period of preservation of the alluvial sediments on a coastal area implies a constant base level after the deposition of the terrace T1 despite the occurrence of an active subduction zone.

Acknowledgements

Support in the laboratory by Julia Krbanjevic is greatly appreciated. The support by Prof. Silvia Rosas and her team (PUCP, Lima) to solve logistic problems at the customs are greatly acknolwedged. This research has been supported by funds of the Swiss National Science Foundation awarded to Schlunegger (project number 155892).

References

Abe-Ouchi, A., Saito, F., Kawamura, K., Raymo, M. E., Okuno, J. I., Takahashi, K., Blatter, H., 2013. Insolation-driven 100,000-year glacial cycles and hysteresis of ice-sheet volume. Nature 500(7461), 190-193.

Akçar, N., Deline, P., Ivy-Ochs, S., Alfimov, V., Hajdas, I., Kubik, P.W., et al., 2012. The 1717 AD rock avalanche deposits in the upper Ferret Valley (Italy): a dating approach with cosmogenic ^{10}Be. Journal of Quaternary Science 27(4), 337–440.

Akçar, N., Ivy-Ochs, S., Alfimov, V., Schlunegger, F., Claude, A., Reber, R., Christl, M., Vockenhuber, C., Dehnert, A., Rahn M., Schlüchter, C. 2017. Isochron-burial dating of glaciofluvial deposits: First results from the Swiss Alps. Earth Surface Processes Landforms. In Press.

Anderson, R.S., Repka, J.L., Dick, G.S., 1996. Explicit treatment of inheritance in dating depositional surfaces using in situ 10Be and 26Al. Geology 24(1), 47-51.

Baker P.A., Seltzer G.O., Fritz, S.C., Dunbar, R.B., Grove, M.J., Tapia, P.M., Cross, S.L., Rowe, H.D., Broda, J.P. 2001a. The history of South American tropical precipitation for the past 25,000 years. Science 291,640–643.

Baker, P.A., Rigsby, C.A., Seltzer, G.O., Fritz, S.C., Lowenstein, T., Bacher, N., Veliz, C. 2001b. Tropical climate changes at millennial and orbital timescales on the Bolivian Altiplano. Nature 409, 698–701.

Balco, G., Rovey, C.W., 2008. An isochron method for cosmogenicnuclide dating of buried soils and sediments. American Journal of Sciences 308, 1083–1114.

Balco, G., Stone, J.O., Lifton, N.A., Dunai, T.J., 2008. A complete and easily accessible means of calculating surface exposure ages or erosion rates from Be-10 and Al-26 measurements. Quarternary Geochronology 3, 174–195.

Bekaddour, T., Schlunegger, F., Vogel, H., Delunel, R., Norton, K. P., Akçar, N., Kubik, P., 2014. Paleo erosion rates and climate shifts recorded by Quaternary cut-and-fill sequences in the Pisco Valley, central Peru. Earth and planetary science letters 390, 103-115.

Bills, B.G., De Silva, S.L., Currey, D.R., Emenger, R.S., Lillquist, K.D., Donnellan, A., Worden, B., 1994. Hydro-isostatic deflection and tectonic tilting in the central Andes: Initial results of a GPS survey of Lake Minchin shorelines. Geophysical Research Letters 21(4), 293-296.

Bookhagen, B., Thiede, R. C., Strecker, M. R., 2005. Abnormal monsoon years and their control on erosion and sediment flux in the high, arid northwest Himalaya. Earth and Planetary Science Letters, 231(1), 131-146.

Bookhagen, B., Fleitmann, D., Nishiizumi, K., Strecker, M. R., Thiede, R. C., 2006. Holocene monsoonal dynamics and fluvial terrace formation in the northwest Himalaya, India. Geology 34(7), 601-604.

Borchers, B., Marrero, S., Balco, G., Caffee, M., Goehring, B., Lifton, N., Nishiizumi, K., Phillips, F., Schaefer, J., Stone, J., 2016. Geological calibration of spallation production rates in the CRONUS-Earth project. Quaternary Geochronology 31, 188–198.

Braucher, R., Merchel, S., Borgomano, J., Bourles, D.L., 2011. Production of cosmogenic radionuclides at great depth: A multi element approach. Earth and Planetary Science Letters 309(1), 1–9.

Chmeleff, J., von Blanckenburg, F., Kossert, K., Jakob, D., 2010. Determination of the Be-10 half-life by multicollector ICP-MS and liquid scintillation counting. Nuclear Instruments and Methods in Physics, Research Section B: Beam Interactions with Materials and Atoms 268.

Christl, M., Vockenhuber, C., Kubik, P.W., Wacker, L., Lachner, J., Alfimov, V., Synal, H.A., 2013. The ETH Zurich AMS facilities: Performance parameters and reference materials. Nuclear Instruments and Methods in Physics Research Section B: Beam Interactions with Materials and Atoms 294, 29-38.

D'arcy, M., Whittaker, A.C., Roda-Boluda, D.C., 2017. Measuring alluvial fan sensitivity to past climate changes using a self-similarity approach to grain-size fining, Death Valley, California. Sedimentology 64(2), 388-424.

Darling, A.L., Karlstrom, K.E., Granger, D.E., Aslan, A., Kirby, E., Ouimet, W. B., Cole, R. D., 2012. New incision rates along the Colorado River system based on cosmogenic burial dating of terraces: Implications for regional controls on Quaternary incision. Geosphere 8(5), 1020-1041.

DeVries, T.J., 1987, A review of geological evidence for ancient El Nino activity in Peru. J. Geophys. Res 92(14), 471–14

Dunne, J., Elmore, D., Muzikar, P., 1999. Scaling factors for the rates of production of cosmogenic nuclides for geometric shielding and attenuation at depth on sloped surfaces. Geomorphology 27, 3–11.

Erlanger, E.D., Granger, D.E., Gibbon, R. J., 2012. Rock uplift rates in South Africa from isochron burial dating of fluvial and marine terraces. Geology 40(11), 1019-1022.

Fritz, S.C., Baker, P.A., Lowenstein, T.K., Seltzer, G.O., Rigsby, C.A., Dwyer, G.S., and Luo, S., 2004, Hydrologic variation during the last 170,000 years in the southern hemisphere tropics of South America: Quarternary Research 61, 95–104, doi: 10 .1016 /j .yqres .2003 .08 .007.

Garreaud, R. D., 2009. The Andes climate and weather. Advances in Geosciences 22, 3.

Garreaud, R., Vuille, M., Clement, A. C., 2003. The climate of the Altiplano: Observed current conditions and mechanisms of past changes. Paleogeography, Paleoclimatology, Paleoecology 194, 5–22.

Gosse, J.C., Phillips, F.M., 2001. Terrestrial in situ cosmogenic nuclides: theory and application. Quaternary Science Reviews 20(14), 1475-1560.

Granger DE. 2006. A review of burial dating methods using 26Al and 10Be. Geological Society of America Special Publication 415, 1-16.

Granger, D.E., Smith, A.L., 2000. Dating buried sediments using radioactive decay and muogenic production of 26Al and 10Be. Nuclear Instruments and Methods in Physics Research, B172, 822-826.

Granger, D.E., Kirchner, J.W., Finkel, R.C., 1996. Spatially averaged long-term erosion rates measured from in situ-produced cosmogenic nuclides in alluvial sediment. Journal of Geology 104, 249-257.

Granger, D.E., Muzikar, P.F., 2001. Dating sediment burial with in situproduced cosmogenic nuclides: theory, techniques, and limitations. Earth and Planetary Science Letters 188, 269–281.

Granger, D.E., Lifton, N.A., Willenbring, J.K., 2013. A cosmic trip: 25 years of cosmogenic nuclides in geology. Geological Society of America Bulletin 125(9-10), 1379-1402.

Hancock, G.S., Anderson, R.S., 2002. Numerical modeling of fluvial strath-terrace formation in response to oscillating climate. Geological Society of America Bulletin 114(9), 1131-1142.

Hidy, A.J., Gosse, J.C., Pederson, J.L., Mattern, J.P., Finkel, R.C., 2010. A geologically constrained Monte Carlo approach to modeling exposure ages from profiles of cosmogenic nuclides: An example from Lees Ferry, Arizona. Geochemistry Geophysics, Geosystems 11.

Kohl, C.P., Nishiizumi, K., 1992. Chemical isolation of quartz for measurement of in-situ-produced cosmogenic nuclides. Geochimica et Cosmochimica Acta 56(9), 3583-3587.

Korschinek, G., Bergmaier, A., Faestermann, T., Gerstmann, U.C., Knie, K., Rugel, G., 2010. A new value for the half-life of Be-10 by heavy-ion elastic recoil detection and liquid scintillation counting. Nuclear Instruments and Methods in Physics Research Section B: Beam Interactions with Materials and Atoms 268, 187-191.

Lagos, P., Silva, Y., Nickl, E., Mosquera, K., 2008. El Niño? related precipitation variability in Perú. Advances in Geosciences 14, 231-237.

Lal, D., 1991. Cosmic-ray labeling of erosion surfaces—In situ nuclide production-rates and erosion models. Earth and Planetary Science Letters 104, 424–439.

Lisiecki, L.E., 2010. Links between eccentricity forcing and the 100,000-year glacial cycle. Nature Geosci. 3, 349–352.

Litty C., Duller R., Schlunegger F., 2016. Paleohydraulic reconstruction of a 40 kyr-old terrace sequence implies that water discharge was larger than today. Earth Surface Processes and Landforms 41, 884-898. DOI: 10.1002/esp.3872.

Litty, C., Lanari, P., Burn, M., Schlunegger, F., 2017a. Climate-controlled shifts in sediment provenance inferred from detrital zircon ages, western Peruvian Andes. Geology 45(1), 59-62.

Litty, C., Schlunegger, F., Viveen, W., 2017b. Possible threshold controls on sediment grain properties of Peruvian coastal river basins. Earth Surface Dynamics 5, 1-13. https://doi.org/10.5194/esurf-5-1-2017

McPhillips, D., Bierman, P.R., Rood, D. H., 2014. Millennial-scale record of landslides in the Andesconsistent with earthquake trigger. Nature Geoscience 7(12), 925-930.

NASA Land Processes Distributed Active Archive Center (LP DAAC). ASTER GDEM. USGS/Earth Resources Observation and Science (EROS) Center, Sioux Falls, South Dakota, 2001.

Norris, T.L., Gancarz, A.J., Rokop, D.J., Thomas, K.W., 1983. Half-life of 26Al. Journal of Geophysical Research, Solid Earth 88(S01).

Norton, K.P., Schlunegger, F., Litty. C., 2016. On the potential for regolith control of fluvial terrace formation in semi-arid escarpments. Earth Surf. Dynam 4, 147-157, https://doi.org/10.5194/esurf-4-147-2016.

Milankovitch, M. Kanon der Erdbestrahlung und seine Anwendung auf das Eiszeitproblem (R. Serbian Acad., 1941).

Pederson, J.L., Anders, M.D., Rittenhour, T.M., Sharp, W.D., Gosse, J. C., Karlstrom, K.E., 2006. Using fill terraces to understand incision rates and evolution of the Colorado River in eastern Grand Canyon, Arizona. Journal of Geophysical Research: Earth Surface 111(F2).

Pillans, B., Chappell, J., Naish, T.R., 1998. A review of the Milankovitch climatic beat: template for Plio–Pleistocene sea-level changes and sequence stratigraphy. Sedimentary Geology 122(1), 5-21.

Placzek, C., Quade, J., Patchett, P.J., 2006. Geochronology and stratigraphy of late Pleistocene lake cycles on the southern Bolivian Altiplano: implications for causes of tropical climate change. Geological Society of America Bulletin 118, 515–532.

Reber, R., Delunel, R., Schlunegger, F., Litty, C., Madella, A., Akçar, N., Christl, M., 2017. Environmental controls on 10Be-based catchment-averaged denudation rates along the western margin of the Peruvian Andes. Terra Nova.

Repka, J.L., Anderson, R.S., Finkel, R.C., 1997. Cosmogenic dating of fluvial terraces, Fremont River, Utah. Earth and Planetary Science Letters 152(1), 59-73.

Steffen, D., Schlunegger, F., Preusser, F., 2009. Drainage basin response to climate change in the Pisco Valley, Peru. Geology 37, 491–494.

Steffen, D., Schlunegger, F., Preusser, F., 2010, Late Pleistocene fans and terraces in the Majes Valley, southern Peru, and their relation to climatic variations. International Journal of Earth Sciences 99(8), 1975-1989.

Stone, J.O., 2000. Air pressure and cosmogenic isotope production. Journal of Geophysical Research: Solid Earth 105(B10), 23753-23759.

Strecker, M.R., Alonso, R.N., Bookhagen, B., Carrapa, B., Hilley, G.E., Sobel, E.R., Trauth, M.H., 2007, Tectonics and climate of the southern central Andes: Annual Review of Earth and Planetary Sciences 35, 747–787, doi: 10 .1146 /annurev .earth .35 .031306 .140158.

Sylvestre, F., Servant, M., Servant-Vildary, S., Causse, C., Fournier, M., Ybert, J. P., 1999. Lake-level chronology on the Southern Bolivian Altiplano (18–23 S) during late-glacial time and the early Holocene. Quaternary Research 51(1), 54-66.

Trauerstein M, Lowick SE, Preusser F, Schlunegger F. 2014. Small aliquot and single grain IRSL and post-IR IRSL dating of fluvial and alluvial sediments from the Pativilca Valley, Peru. Quaternary Geochronology 112, 163–174.

Tucker GE, Slingerland R. 1997. Drainage basin response to climate change. Water Resources Researc. 33, 2031–2047.

Veit, H., May, J.H., Madella, A., Delunel, R., Schlunegger, F., Szidat, S., Capriles, J. M., 2016. Palaeo- geoecological significance of Pleistocene trees in the Lluta Valley, Atacama Desert. Journal of Quaternary Science 31(3), 203-213.

Von Blanckenburg F. 2005. The control mechanisms of erosion and weathering at basin scale from cosmogenic nuclides in river sediment. Earth and Planetary Science Letters 237(3), 462–479.

Wolkowinsky, A.J., Granger, D.E., 2004. Early Pleistocene incision of the San Juan River, Utah, dated with 26Al and 10Be. Geology 32(9), 749-752.

Tables and Figures captions

Table 1: Sample and cosmogenic nuclide data.

Table 2: Input parameters for the Monte Carlo simulator in Matlab® (Hidy et al., 2010).

Table 3: Results of the Monte Carlo simulations with Matlab® for (A) Barranca and (B) Pativilca. Total number of simulated profiles is 100,000. The bold numbers represent the modelled values and are therefore the ones that are used in this paper.

Table 4: Information relevant for interpreting ^{10}Be concentrations. Modern and paleo catchment-averaged denudation were calculated using the SRTM DEM with a 90 m resolution. A ^{10}Be half-life of 1.39 +/- 0.01 Ma was used (Chmeleff et al., 2010; Korschinek et al., 2010) and a SLHL ^{10}Be production rate of 4.01 at g^{-1} a^{-1}. A density of 2.65 g cm^{-3} was employed.

Fig. 1: (A) Maps of the study area showing the location of Pativilca and Barranca on the western side of the Peruvian Andes. (B) Field photographs showing the alluvial terraces in Barranca and Pativilca. Samples PAT-DP-1 to 6 (Pativilca), BAR-DP 1 to 6 (Barranca) were collected for depth-profile dating. The white lines represent the bracket level where quartz bearing clasts were sampled for isochron burial dating purposes. The concentrations obtained for the samples BAR-DP6 and PAT-DP6 were used for the calculation of the paleo-basin wide denudation rates

Fig. 2: Measured ^{26}Al concentrations plotted vs. ^{10}Be concentrations of the isochron-burial dating samples in Barranca (BAR-IS1, BAR-IS2 and BAR-IS3) and in Pativilca (PAT-IS1 and PAT-IS2). The sampling sites are shown on Fig. 1B. The errors represent 2σ uncertainties. The dash lines illustrate the surface production rate ratio of 6.75 (Balco et al., 2008).

Fig. 3: Measured ^{10}Be concentrations including the 1σ uncertainties of the Barranca depth-profile samples plotted against depth.

Fig. 4: Modal output of the Monte Carlo simulations showing frequency distributions and $\chi 2$ values for exposure age, erosion rate and inheritance.

Fig. 5: Output of the Monte Carlo depth-profile age simulation. (A) Illustration of the best fit through the samples for the lowest $\chi 2$ value. (B) Possible solution space with a $\chi 2$ cut-off values of < 20.

Fig. 6: Measured ^{10}Be concentrations including the 1σ uncertainties of the Pativilca depth-profile samples plotted against depth.

Fig. 7: Modal output of the Monte Carlo simulations showing frequency distributions and $\chi 2$ values for exposure age, erosion rate and inheritance.

Fig. 8: Output of the Monte Carlo depth-profile age simulation. (A) Illustration of the best fit through the samples for the lowest $\chi 2$ value. (B) Possible solution space with a $\chi 2$ cut-off values of < 3.

Fig. 9: Map of the alluvial terraces in Pativilca and Barranca showing the age of the different terraces.

Fig. 10: (A) Summary of the IRSL and depth-profile ages in Pativilca and Barranca. The black dots represent the IRSL samples from Trauerstein et al. (2014) and the white dot represents the depth profile (this study). (B) Summary of the paleo-catchment wide denudation rates.The transect A-B can be seen in Fig. 9.

Fig. 11: Maps showing the inferred channel belt position during the sediment accumulation phases in the Pativilca Valley. (A) prior to ~1.2 Ma ago. (B) prior to ~200 ka ago. (C) ~100 ka ago. (D) ~30 ka ago.

Fig. 12: Erosion rates versus time.

Figur
e 1

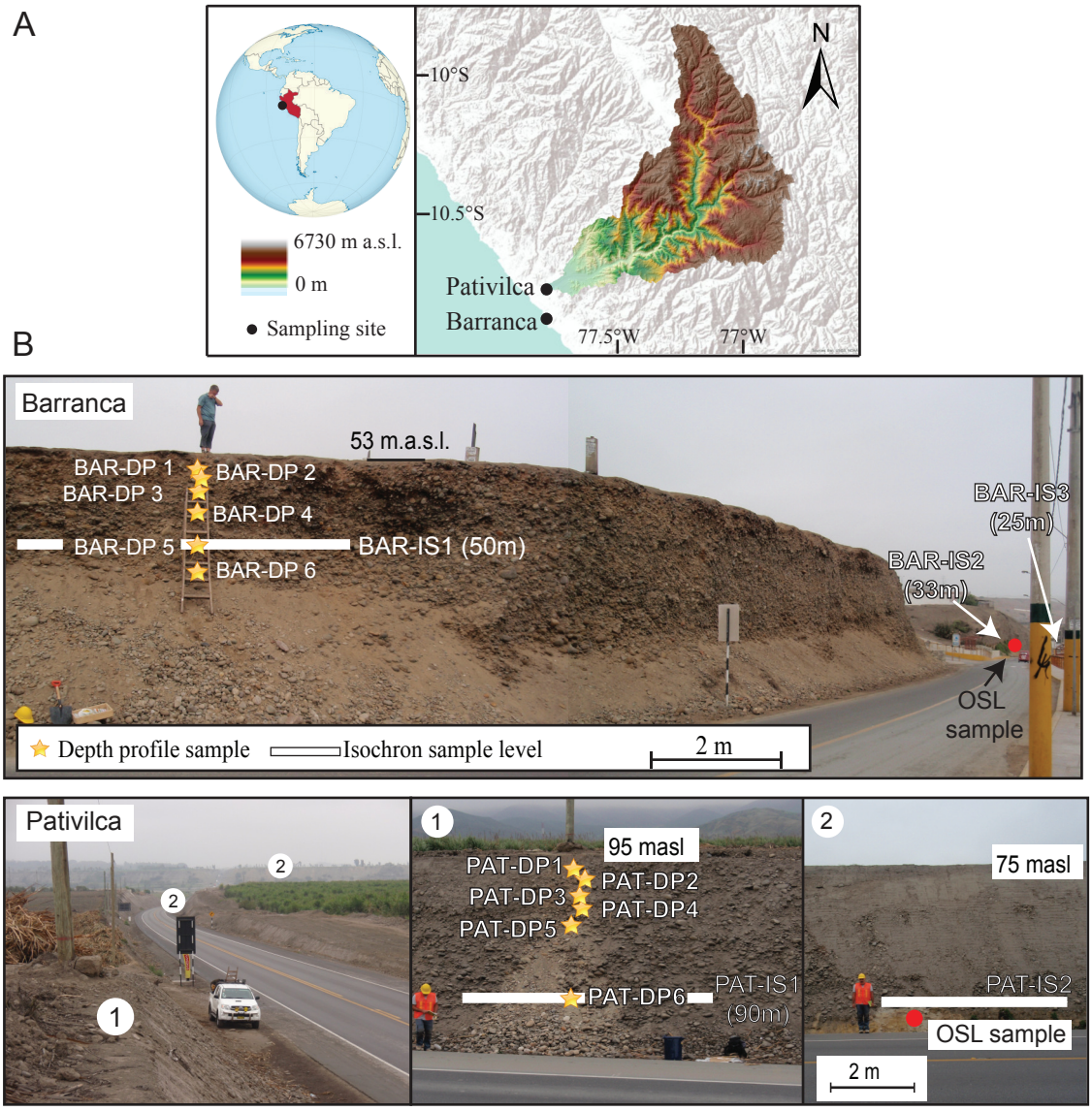
A
6730 m a.s.l.
0 m
Sampling site
10°S
10.5°S
N
Pativilca
Barranca
77.5°W
77°W
B
Barranca
53 m.a.s.l.
BAR-DP 1
BAR-DP 2
BAR-DP 3
BAR-DP 4
BAR-DP 5
BAR-IS1 (50m)
BAR-DP 6
BAR-IS3
(25m)
BAR-IS2
(33m)
OSL
sample
Depth profile sample
Isochron sample level
2 m
Pativilca
1
2
95 masl
PAT-DP1
PAT-DP2
PAT-DP3
PAT-DP4
PAT-DP5
PAT-DP6
PAT-IS1
(90m)
75 masl
PAT-IS2
OSL sample
2 m

Figur
e 2

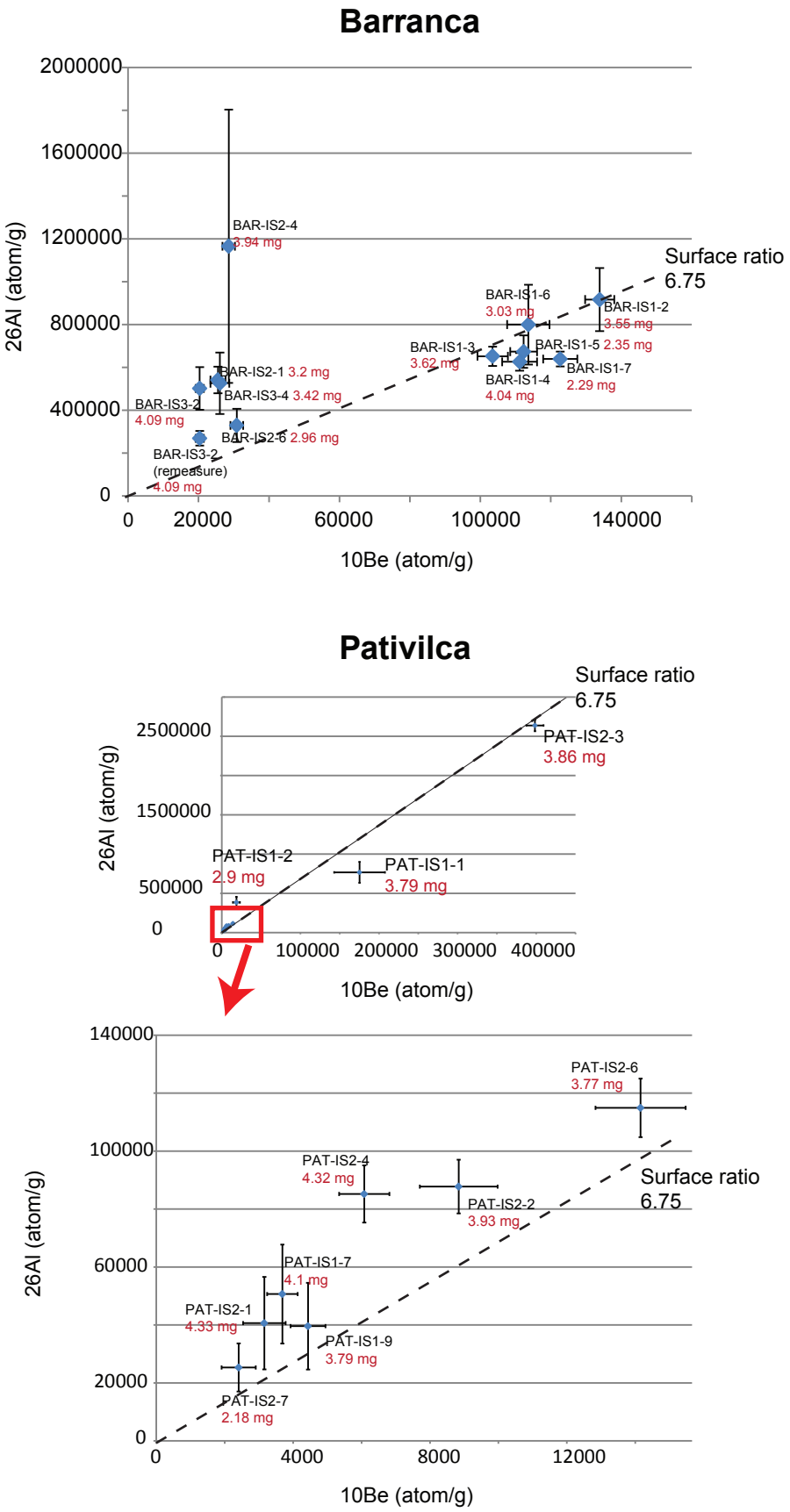
Barranca
2000000
1600000
1200000
800000
400000
0
26Al (atom/g)
0
20000
60000
100000
140000
10Be (atom/g)
Surface ratio
6.75
BAR-IS2-4
3.94 mg
BAR-IS1-6
3.03 mg
BAR-IS1-2
3.55 mg
BAR-IS1-3
3.62 mg
BAR-IS1-5 2.35 mg
BAR-IS1-4
4.04 mg
BAR-IS1-7
2.29 mg
BAR-IS2-1 3.2 mg
BAR-IS3-4 3.42 mg
BAR-IS3-2
4.09 mg
BAR-IS2-5 2.96 mg
BAR-IS3-2
(remeasure)
4.09 mg
Pativilca
Surface ratio
6.75
2500000
1500000
500000
0
26Al (atom/g)
PAT-IS2-3
3.86 mg
PAT-IS1-2
2.9 mg
PAT-IS1-1
3.79 mg
0
100000
200000
300000
400000
10Be (atom/g)
140000
100000
60000
20000
0
26Al (atom/g)
PAT-IS2-6
3.77 mg
PAT-IS2-4
4.32 mg
PAT-IS2-2
3.93 mg
Surface ratio
6.75
PAT-IS1-7
4.1 mg
PAT-IS2-1
4.33 mg
PAT-IS1-9
3.79 mg
PAT-IS2-7
2.18 mg
0
4000
8000
12000
10Be (atom/g)

Barranca Depth Profile (Peru)

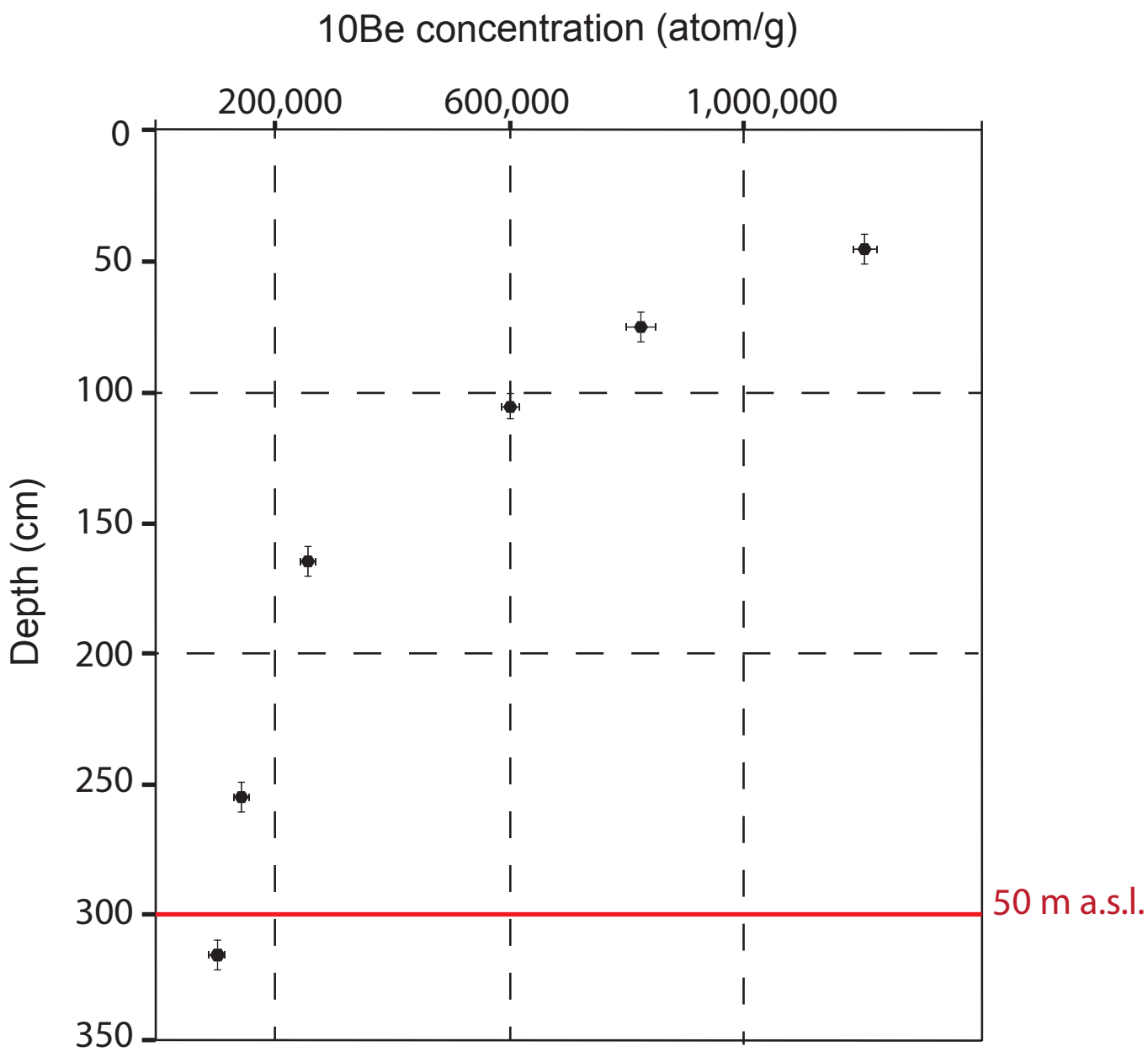

Figur
e 4

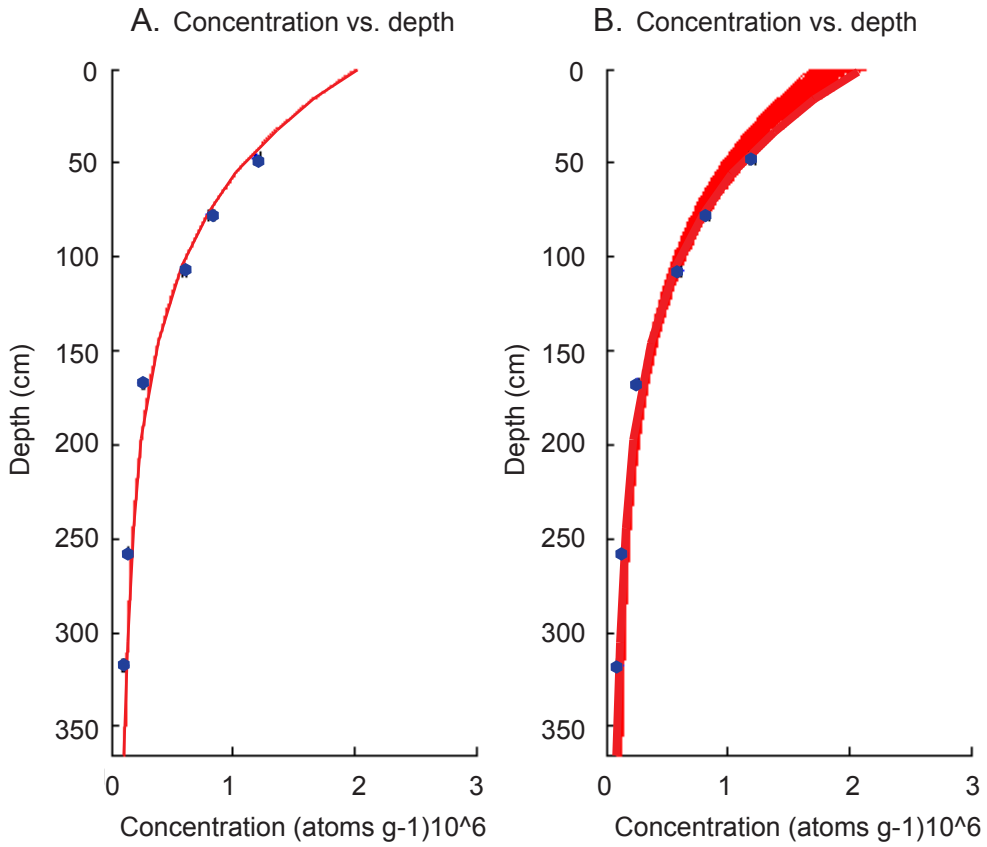
A. Concentration vs. depth
B. Concentration vs. depth
Depth (cm)
0
50
100
150
200
250
300
350
0
1
2
3
Concentration (atoms g-1)10^6

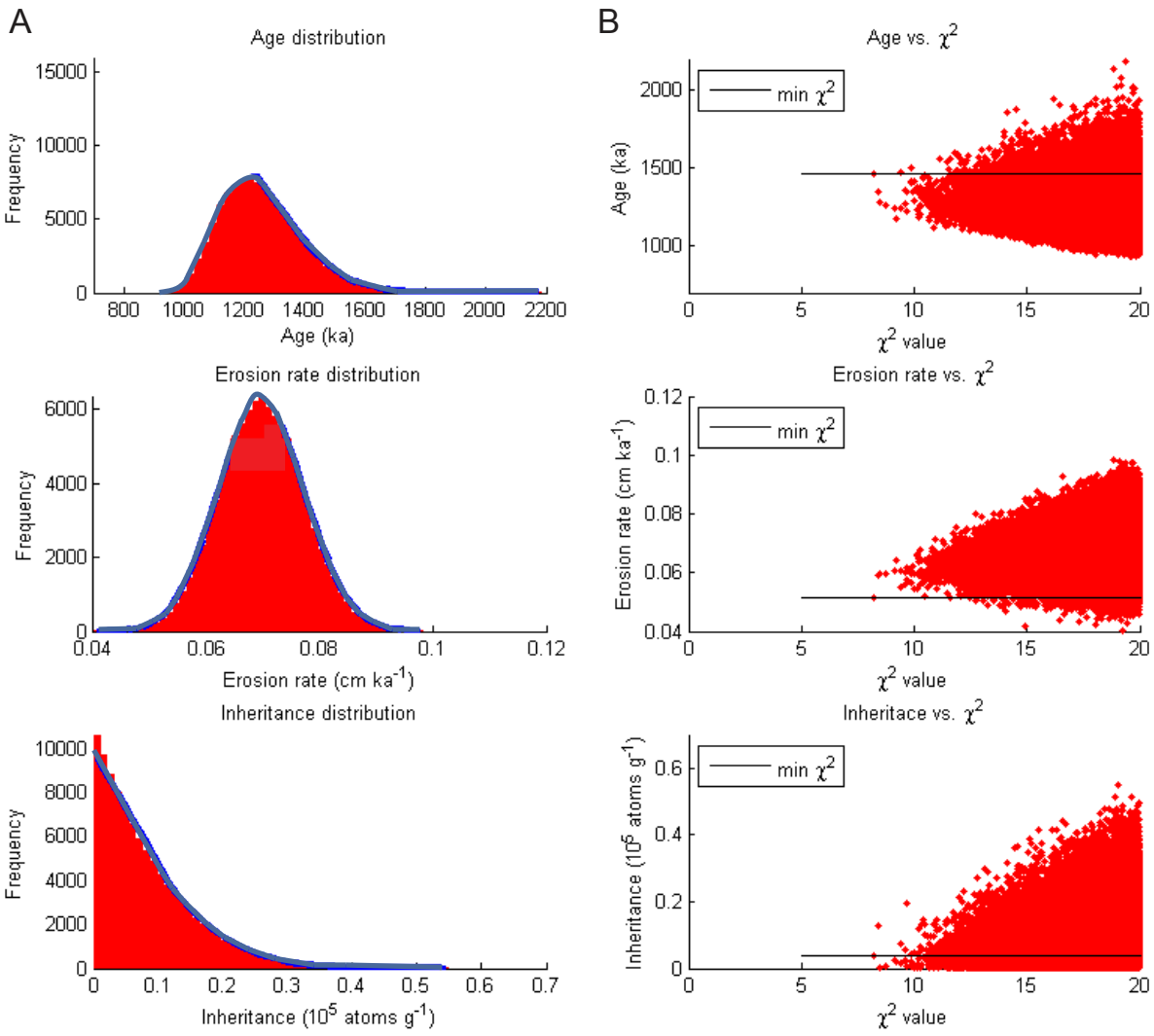
A
Age distribution
Frequency
Age (ka)
Erosion rate distribution
Erosion rate (cm ka-1)
Inheritance distribution
Inheritance (10^5 atoms g^-1)
B
Age vs. χ2
min χ2
Age (ka)
χ2 value
Erosion rate vs. χ2
Erosion rate (cm ka-1)
Inheritace vs. χ2
Inheritance (10^5 atoms g-1)

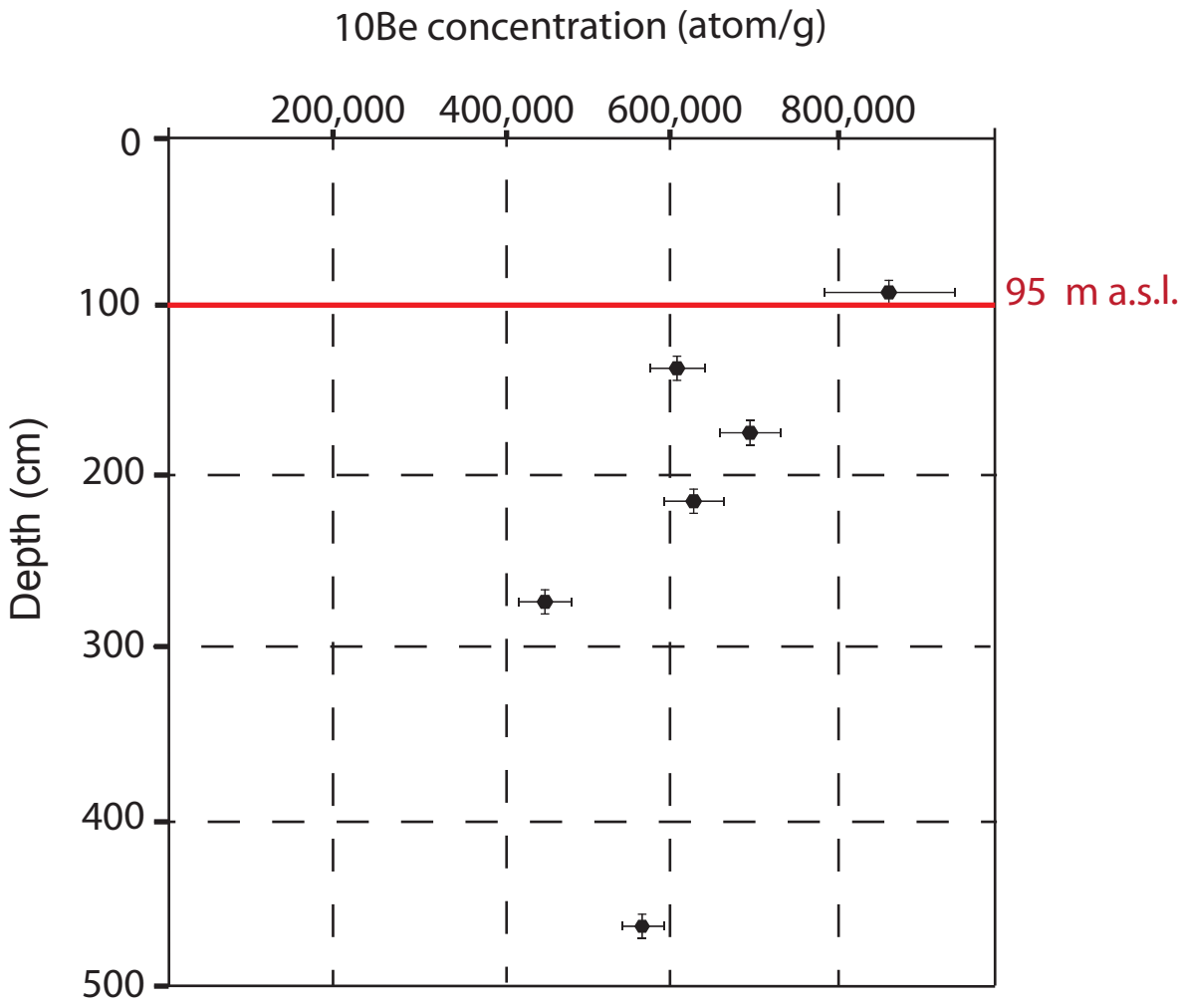
10Be concentration (atom/g)
200,000
400,000
600,000
800,000
0
100
200
300
400
500
Depth (cm)
95 m a.s.l.

Figur
e 7

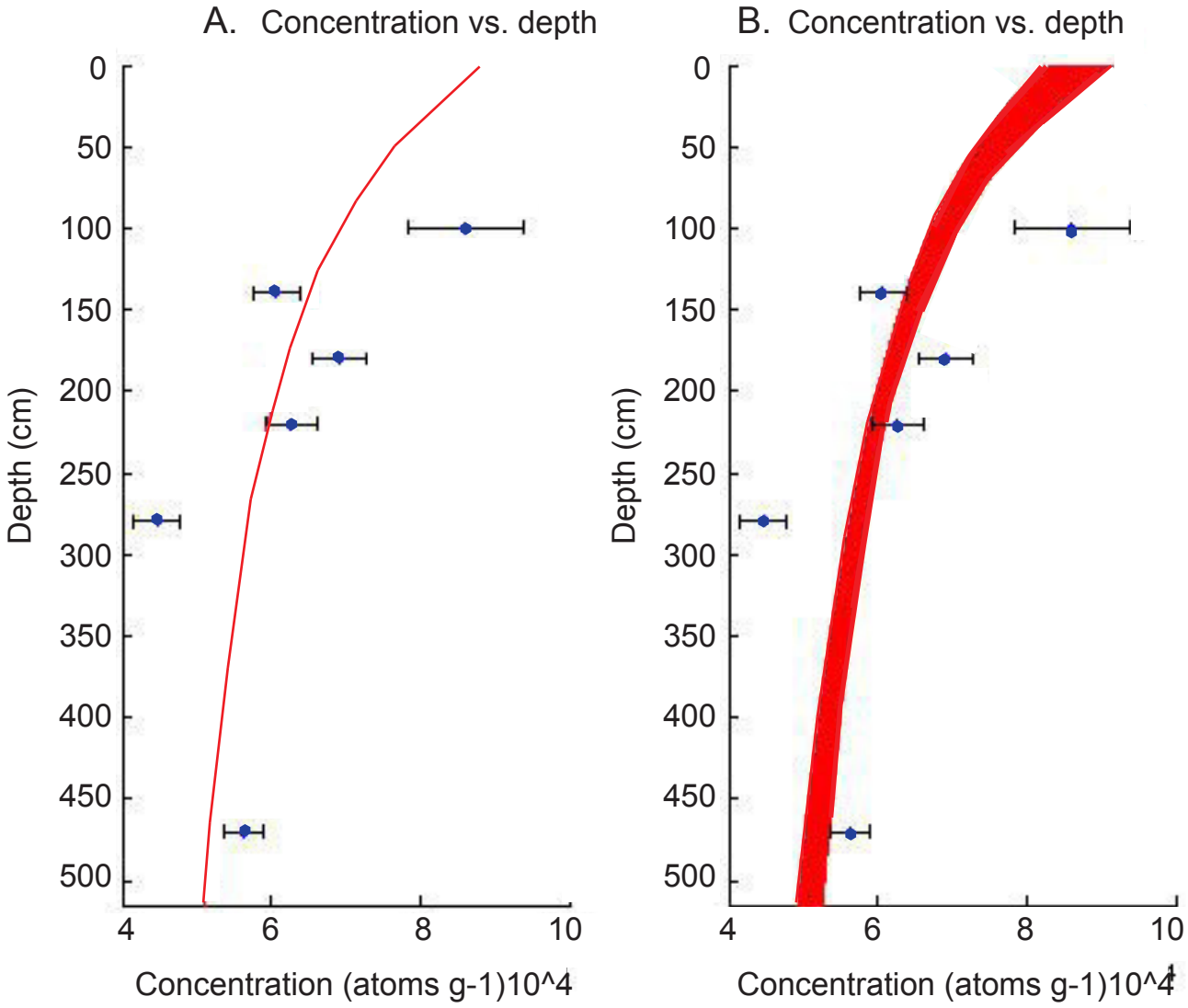
A. Concentration vs. depth
B. Concentration vs. depth
Depth (cm)
0
50
100
150
200
250
300
350
400
450
500
4
6
8
10
Concentration (atoms g-1)10^4

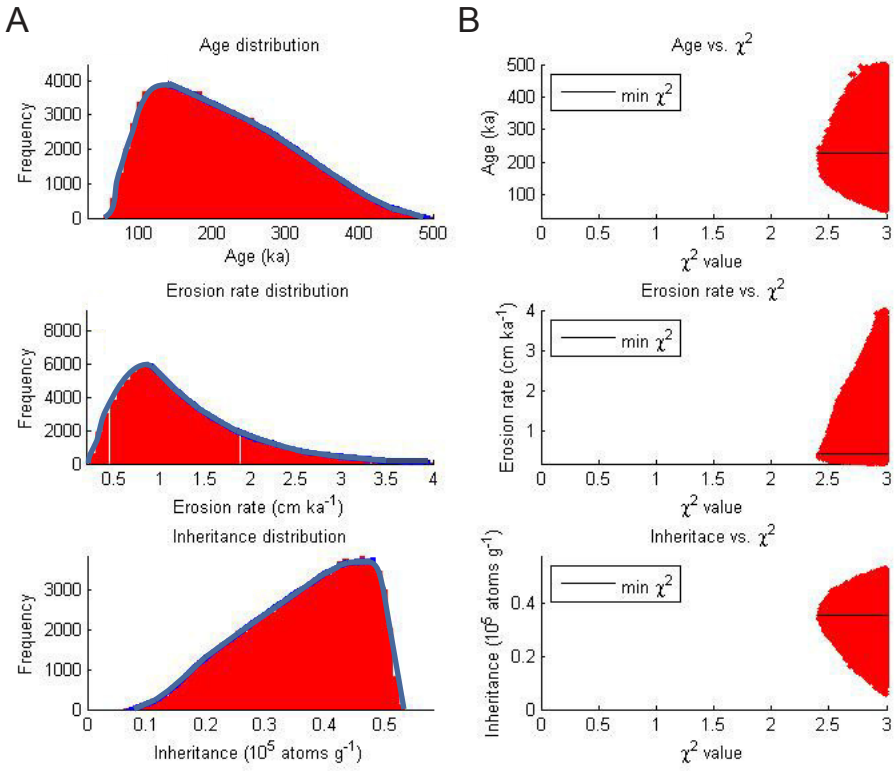
A
Age distribution
Frequency
Age (ka)
Erosion rate distribution
Erosion rate (cm ka-1)
Inheritance distribution
Inheritance (10^5 atoms g^-1)
B
Age vs. χ2
min χ2
Age (ka)
χ2 value
Erosion rate vs. χ2
Erosion rate (cm ka-1)
Inheritace vs. χ2
Inheritance (10^5 atoms g-1)

Figure 9

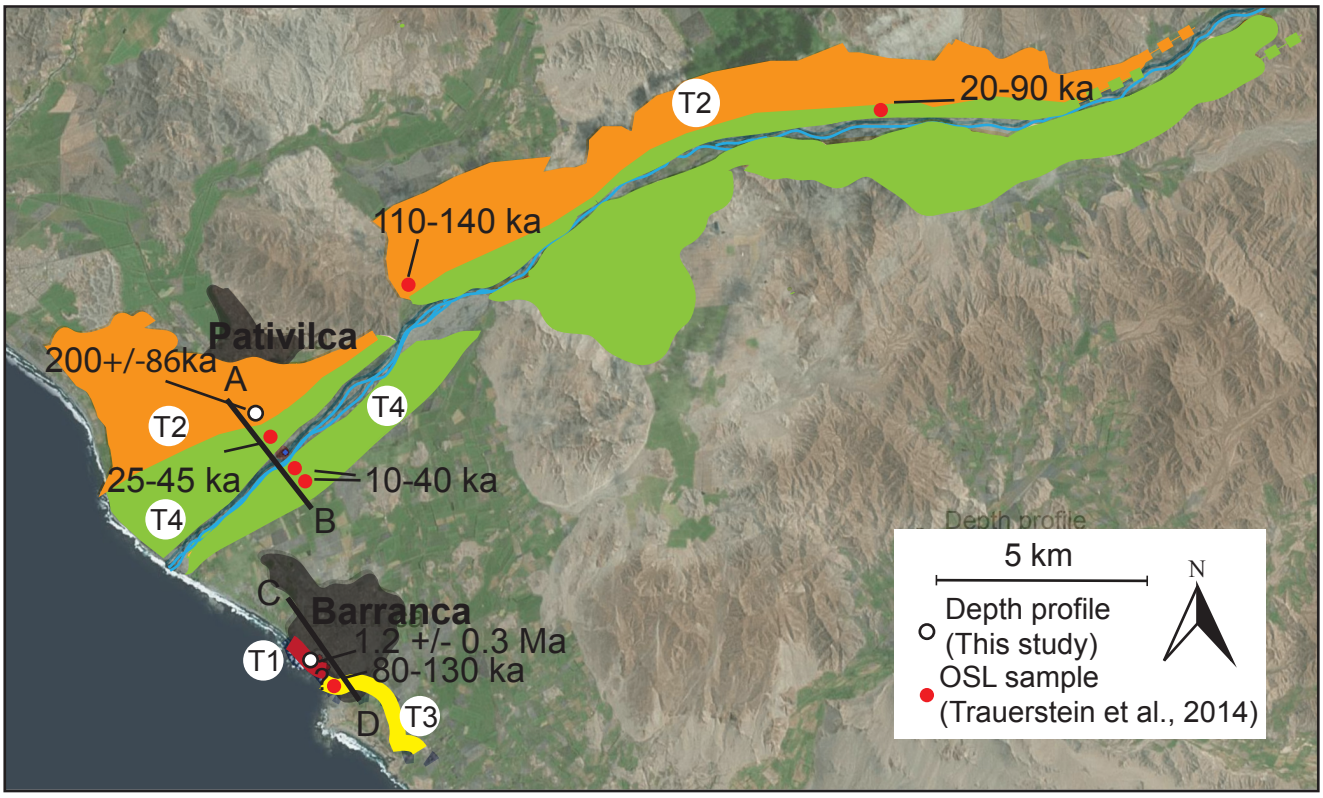
T2
20-90 ka
110-140 ka
Pativilca
200+/-86ka
A
T2
T4
25-45 ka
10-40 ka
T4
B
C
Barranca
1.2 +/- 0.3 Ma
T1
80-130 ka
D
T3
Depth profile
5 km
N
Depth profile
(This study)
OSL sample
(Trauerstein et al., 2014)

Figure 10

A. Ages

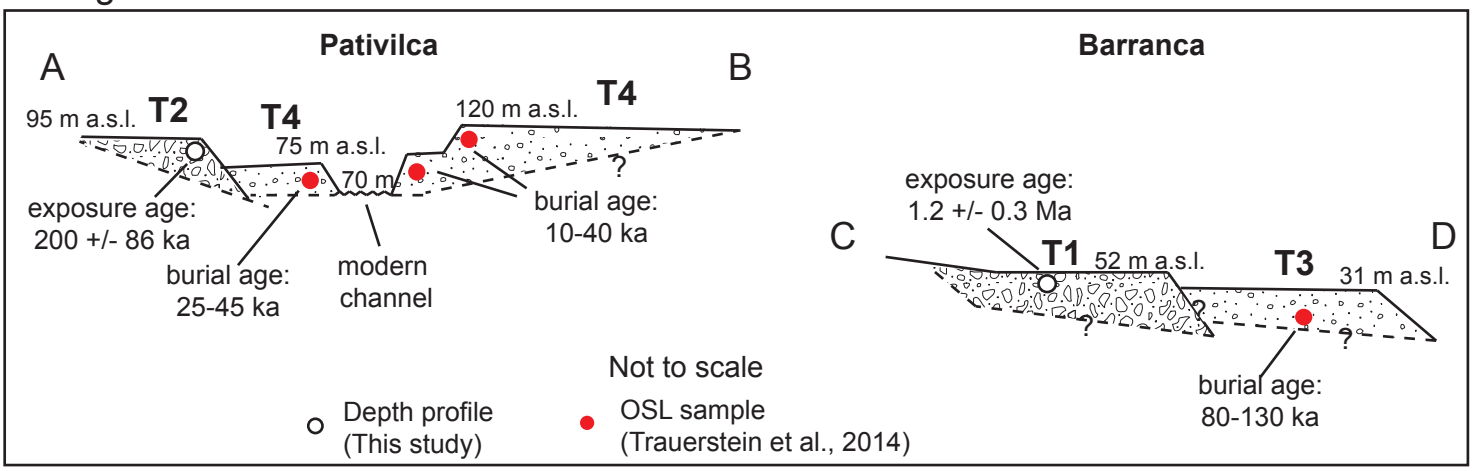

B. Erosion rates

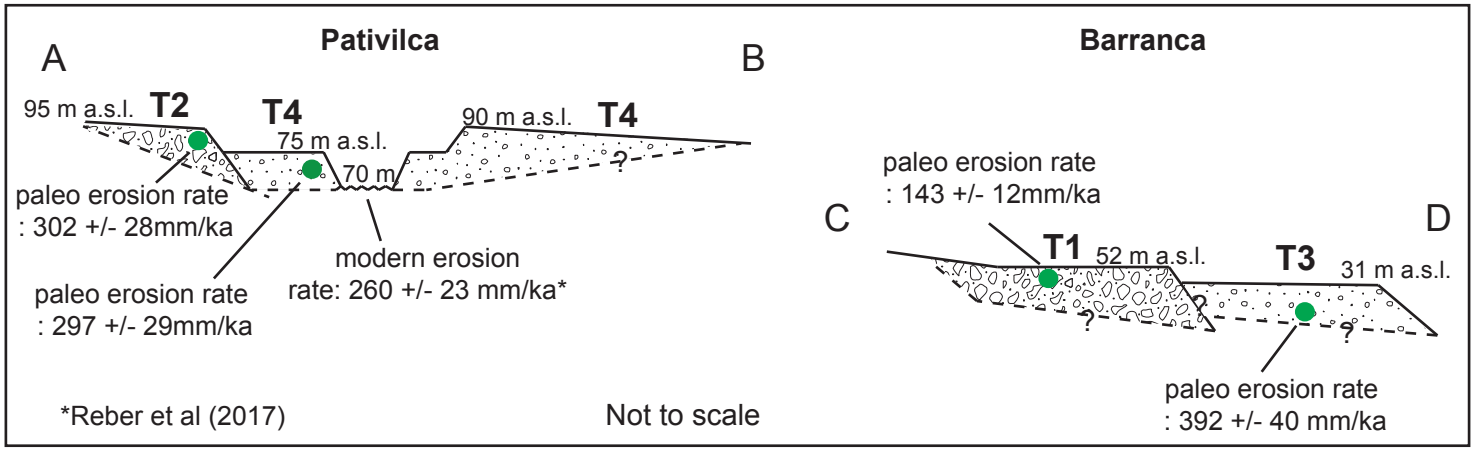

Figure
11

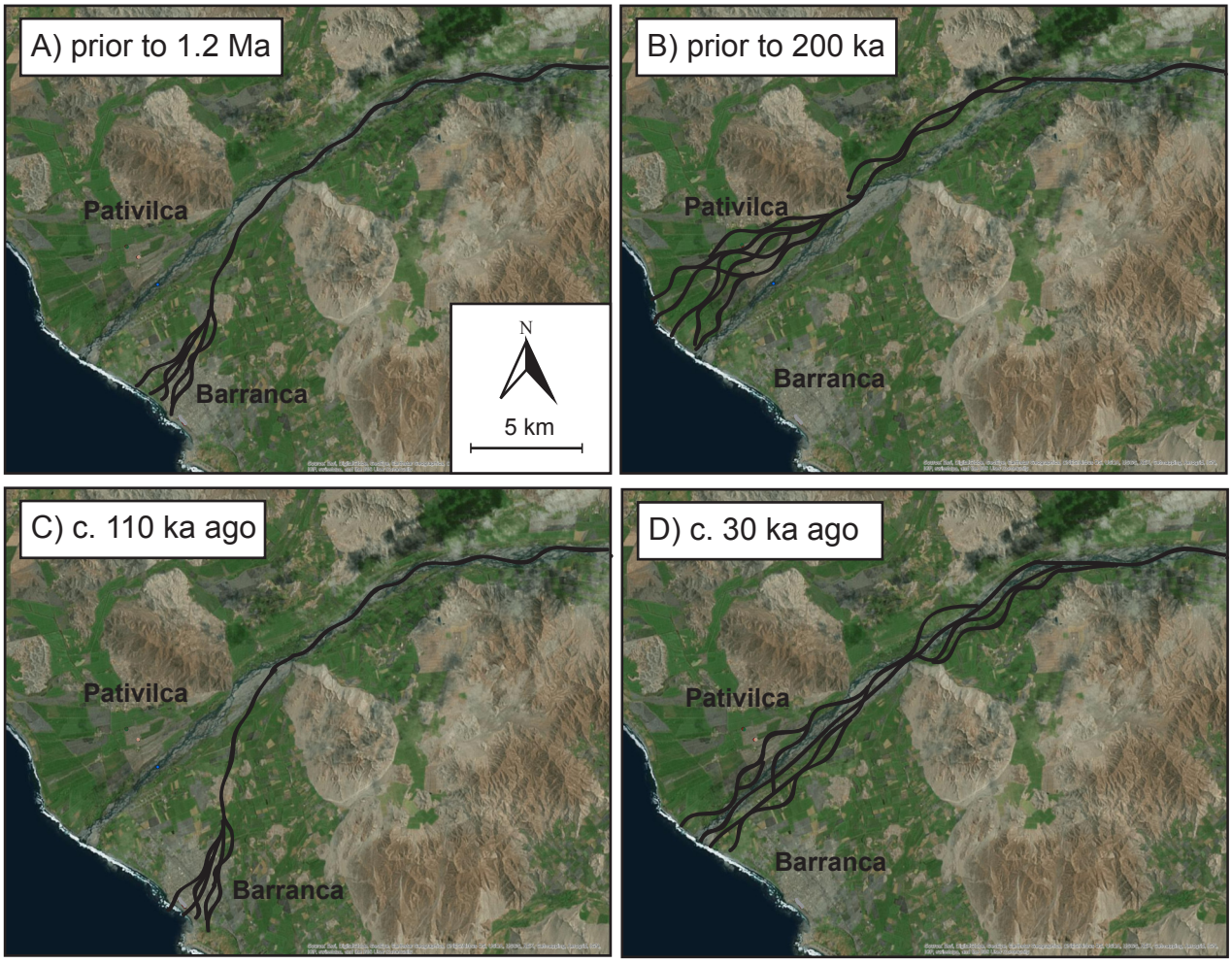
A) prior to 1.2 Ma
Pativilca
Barranca
N
5 km
B) prior to 200 ka
Pativilca
Barranca
C) c. 110 ka ago
Pativilca
Barranca
D) c. 30 ka ago
Pativilca
Barranca

Figure 12

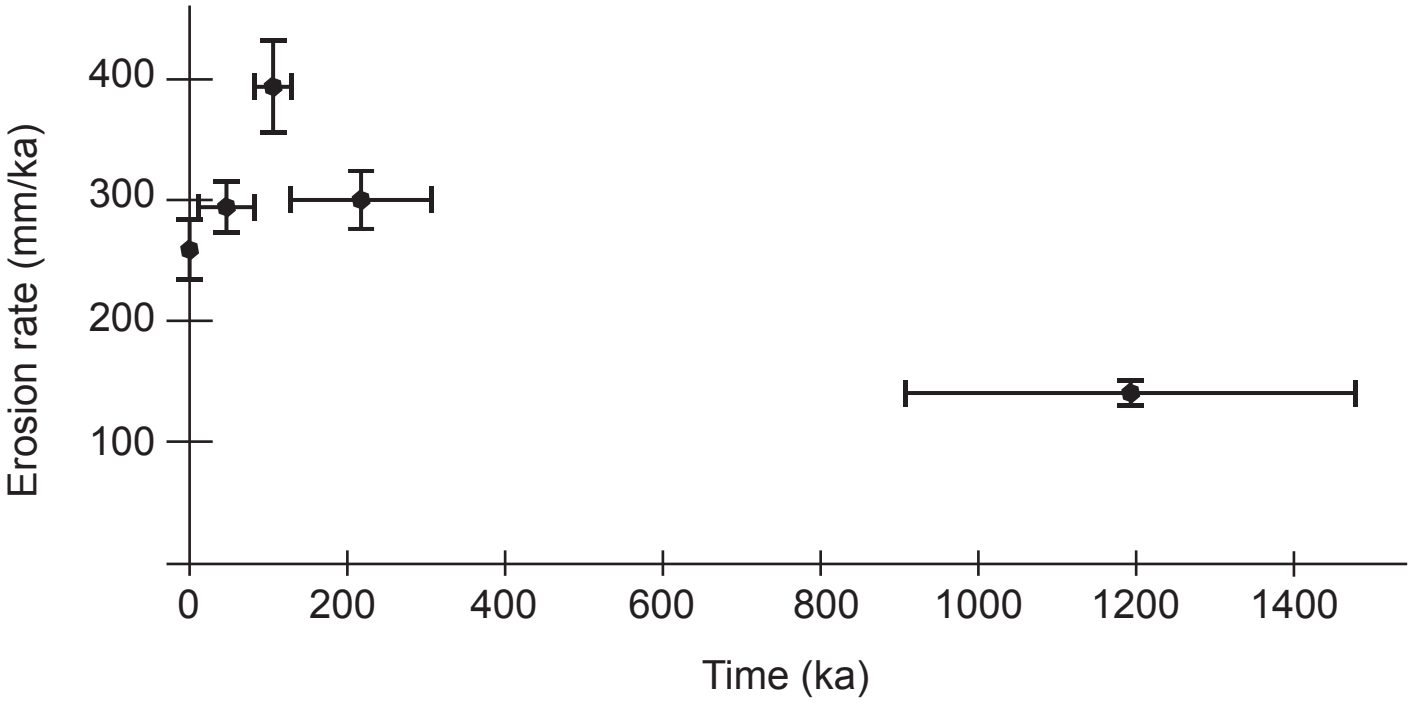
Erosion rate (mm/ka)
400
300
200
100
0
200
400
600
800
1000
1200
1400
Time (ka)

Table 1.

Sample information and cosmogenic nuclide data of the samples

Site	Technics	Latitude (°)	Longitude (°)	Altitude of the top of the terrace (m)	Sample name	Sample depth(cm)	Sample type	Quartz dissolved(g)	9Be spike(mg)	10Be/9Be	Relative uncertainty(%)	10Be concentration (10^4 atoms/g)	Al(mg)	26Al/27Al	Relative uncertainty(%)	26Al concentration (10^4 atoms/g)	26Al/10Be	Error on the ratio
Pativilca	Depth Profile dating	-10.704	-77.775	96	PAT-DP1	90-100	Sand	15.0271	0.1731	1,14E-13	8.72	8.59	n.d	n.d.	n.d.	n.d.	n.d.	n.d.
					PAT-DP2	130-140		49.8738	0.1702	2,68E-13	5.23	6.06						
					PAT-DP3	170-180		49.8325	0.1745	2,98E-13	5.18	6.91						
					PAT-DP4	210-220		50.0394	0.175	2,71E-13	5.38	6.26						
					PAT-DP5	270-280		49.9998	0.1725	1,96E-13	7.08	4.46						
					PAT-DP6	460-470		49.8804	0.1743	2,43E-13	4.64	5.62						
	Isochron burial dating	-10.704	-77.775	96	PAT-IS1-1	460-470	Quartz bearing clasts	38.207	0.1739	5,79E-13	18.4	17.5	3.79	3,46E-13	17,5	76.7	4.38	1.11
					PAT-IS1-2			38.7454	0.1737	6,45E-14	22.9	1.86	2.90	2,30E-13	18,6	38.5	20.7	6.24
					PAT-IS1-7			36.6074	0.1747	1,40E-14	9.96	0.368	4.10	2,03E-14	33,7	5.07	13.8	4.92
					PAT-IS1-9			37.689	0.1746	1,68E-14	9.81	0.443	3.79	1,76E-14	37,8	3.96	8.92	3.52
	Isochron burial dating	-10.708	-77.772	75	PAT-IS2-1	400-410	Quartz bearing clasts	39.5056	0.1737	1,32E-14	16.0	0.315	4.33	1,66E-14	39,3	4.06	12.8	5.65
					PAT-IS2-3			40.9181	0.1739	1,41E-12	2.73	3.98	3.86	1,25E-12	2,78	263	6.62	0.26
					PAT-IS2-7			36.3518	0.175	9,91E-15	15.6	0.241	2.18	1,89E-14	32,8	2.53	10.5	4.08
					PAT-IS2-2			32.5973	0.2004	2,39E-14	11.5	0.884	3.94	3,25E-14	10,6	8.77	9.93	1.65
					PAT-IS2-4			39.2653	0.1972	2,05E-14	10.6	0.608	4.32	3,47E-14	11,6	8.52	14.0	2.34
					PAT-IS2-6			39.8664	0.1998	4,47E-14	8.79	1.41	3.78	5,44E-14	8,79	11.5	8.12	1.04
Barranca	Depth Profile dating	-10.758	-77.765	53	BAR-DP1	40-50	Sand	36.2984	0.1661	3,94E-12	1.54	12.0	n.d	n.d.	n.d.	n.d.	n.d.	n.d.
					BAR-DP2	70-80		33.0576	0.1673	2,43E-12	3.04	82.1						
					BAR-DP3	100-110		25.7899	0.1731	1,34E-12	2.52	60.1						
					BAR-DP4	160-170		35.9971	0.1705	8,31E-13	3.02	26.2						
					BAR-DP5	250-260		50.2153	0.1747	6,08E-13	5.27	14.1						
					BAR-DP6	310-320		33.2556	0.1744	2,96E-13	4.41	10.3						
	Isochron burial dating	-10.758	-77.765	53	BAR-IS1-2	250-260	Quartz bearing clasts	37.67	0.1736	4,37E-13	3.07	13.4	3.55	4,35E-13	16.0	91.6	6.84	1.12
					BAR-IS1-5			25.9268	0.1718	2,36E-13	4.15	10.3	3.62	2,98E-13	6.92	65.2	6.30	0.71
					BAR-IS1-6			32.4907	0.1741	3,13E-13	4.44	11.1	4.05	2,85E-13	6.58	62.6	5.63	1.68
					BAR-IS1-3			37.025	0.2017	3,11E-13	3.38	11.2	2.36	3,32E-13	11.3	67.3	5.99	0.51
					BAR-IS1-4			41.1355	0.2023	3,48E-13	5.25	11.3	3.04	3,83E-13	23.3	79.9	7.03	0.45
					BAR-IS1-7			26.5406	0.2033	2,42E-13	3.91	12.3	2.29	3,31E-13	5.38	63.9	5.21	0.35
	Isochron burial dating	-10.759	-77.764		BAR-IS2-1	< 20 m	Quartz bearing clasts	40.3743	0.1737	9,12E-14	8.10	2.55	3.20	3,06E-13	11.5	54.1	21.2	3.02
					BAR-IS2-4			44.6497	0.1715	1,14E-13	5.99	2.85	3.94	5,91E-13	54.7	116,00	40.8	22.47
					BAR-IS2-6			37.5191	0.1742	1,02E-13	5.63	3.08	2.96	1,86E-13	23.5	32.9	10.6	2.58
	Isochron burial dating	-10.76	-77.763		BAR-IS3-2	< 25 m	Quartz bearing clasts	49.9169	0.1726	9,04E-14	5.68	2.03	4.09	2,74E-13	19.7	50.1	24.7	5.09
					BAR-IS3-4			45.1403	0.1737	1,04E-13	10.11	2.61	3.42	3,11E-13	27.3	52.6	20.2	5.89
					BAR-IS3-7			40.7863	0.1729	7,10E-14	8.56	1,94	3.62	2,79E-13	25.5	55.3	28.4	7.68

Table 2

Input parameters for the Monte Carlo simulator in Matlab (Hidy et al., 2010).

Barranca

Parameter	Value
Latitude (degree)	-10,758
Longitutde (degree)	-77,765
Altitude (m)	53
Strike (degree)	0
Dip (degree)	0
Shielding correction factor	1
Cover correction factor	1
Uncertainty of 10Be Half-life (%)	1
Local spallogenic production rate (at g-1 a-1)	2,50
Error in local spallogenic production rate (at g-1 a-1)	± 0.5
Depth of muon fit (m)	6
Error in total production rate (%)	5
Density (g cm-3)	1.6-2.1
X2 value	20
Numbers of profiles	100,000
Age (a)	700,000-2,200,000
Erosion rate (cm ka-1)	0.04-0.12
Total erosion threshold (cm)	75-400
Inheritance (at g-1)	0-70,000
Attenuation length (g cm-2)	160 ± 5

Pativilca

Parameter	Value
Latitude (degree)	-10,704
Longitutde (degree)	-77,776
Altitude (m)	96
Strike (degree)	0
Dip (degree)	0
Shielding correction factor	1
Cover correction factor	1
Uncertainty of 10Be Half-life (%)	1
Local spallogenic production rate (at g-1 a-1)	2,50
Error in local spallogenic production rate (at g-1 a-1)	± 0.5
Depth of muon fit (m)	6
Error in total production rate (%)	5
Density (g cm-3)	1.6-2.1
X2 value	3
Numbers of profiles	100,000
Age (a)	30,000-500,000
Erosion rate (cm ka-1)	0.2-4
Total erosion threshold (cm)	75-400
Inheritance (at g-1)	0-58,000
Attenuation length (g cm-2)	160 ± 5

A

Table Barranca

Results of the Monte Carlo simulations with Matlab

	Age (ka)	Inheritance (atom/g)	Erosion rate (cm/ka)
Mean	1254.3	8300	0.07
Median	1239.4	6400	0.07
Mode	**1197.1**	**300**	**0.07**
Minimum X2	1261.5	1200	0.06
Maximum	1503.0	5,8000	0.09
Minimum	1043.2	0	0.05

B

Table Pativilca

Results of the Monte Carlo simulations with Matlab

	Age (ka)	Inheritance (atom/g)	Erosion rata (cm/ka)
Mean	200.6	3,5500	0.52
Median	200.3	3,5500	0.51
Mode	**204.1**	**3,5100**	**0.48**
Minimum X2	217.6	3,7800	0.35
Maximum	314.3	4,3800	0.89
Minimum	125	2,7100	0.25

Sample name	Paleo/modern erosion rates	Age of the deposits	Latitude (DD.DD) WGS84	Longitude (DD.DD) WGS84	Altitude of the top of the terrace (m.a.s.l)	Sample depth (cm)	Quartz dissolved (g)	9Be spike (mg)	Measured 10Be/9Be ratio (10^-12)	AMS error (%)	10Be concentration (at/g)	Concentration at the time of deposition (at/g)	Denudation rates (mm/ka)
PAT-ME	Modern erosion rates	Modern Pativilca river	10.717°S	77.767°W	71	Surface	50.11	0.1991	0.24	4.0	6,4052 +/- 2695	6,4052 +/- 2695	260 +/- 23
PAT-DP6	Paleo erosion rates	Terrace T1 (Pativilca) : 200 ka	10.704°S	77.775°W	95	465 cm	49.88	0.1743	0.24	4.6	5,6219 +/- 2634	5,5203 +/- 2539	302 +/-28
PAT-PE	Paleo erosion rates	Terrace T3 (Pativilca) : 40 ka	10.708°S	77.772°W	75	400 cm	49.97	0.1953	0.22	5.5	5,6468 +/- 3144	5,6004 +/- 3080	297 +/- 29
BAR-DP6	Paleo erosion rates	Terrace (Barranca) : 1.2 Ma	10.758°S	77.765°W	52	315 cm	33.25	0.1744	0.30	4.4	10,2942 +/- 4574	11,6020 +/- 2464	143 +/- 12
BAR-PE2	Paleo erosion rates	Terrace (Barranca) : 100 ka	10.759°S	77-764°W	33	400 cm	41.24	0.1984	0.14	6.3	4,4416 +/- 2823	4,2570 +/- 2682	392 +/- 40